

Microstructures of Bimetallic Clusters: Bond Order Metal Simulator for Disordered Alloys

Ling Zhu* and Andrew E. DePristo*†

*Ames Laboratory, U.S. Department of Energy, and †Department of Chemistry, Iowa State University, Ames, Iowa 50011

Received October 3, 1996; revised December 23, 1996; accepted December 23, 1996

Experimental bulk mixing data on disordered bimetallics of Ni, Cu, Rh, Pd, Ag, Ir, Pt, and Au are used to parametrize the recently developed bond order metal simulator (BOS-mixing) model, including a full error analysis. This model characterizes the variation of metal–metal bond strength with number and type of atomic neighbors. The model is shown to accurately fit experimental mixing energy curves as a function of composition irrespective of whether the curves are symmetric or asymmetric around the 50% value. As an illustration of the utility of the BOS-mixing model, we predict the microstructures of bimetallic clusters with 201 atoms (or 61% dispersion) and a composition of 50%–50%. The examples demonstrate how differences in surface energy, mixing energy, and mixing entropy either compete or cooperate in determining the microstructure of small bimetallic clusters.

© 1997 Academic Press

I. INTRODUCTION

Bimetallic catalysts are widely used in the automobile and petroleum industries, e.g., to transform hydrocarbons, manufacture nitric acid, and simultaneously convert carbon monoxide, hydrocarbons, and nitrogen oxides in automobile exhaust (1–6). Compared to monometallic catalysts, bimetallic catalysts are superior in activity, selectivity, and stability. For example, in catalytic reforming of naphtha, bimetallic Pt-based systems appear much better than traditional monometallic Pt catalysts (7). Of these three advantages, enhanced selectivity is perhaps the most desirable, and the goal of promoting a catalyst's activity for a desirable reaction and/or hindering the catalyst's activity for undesirable reactions has been a challenge for many years.

In principle, a bimetallic catalyst can enhance selectivity in two ways: (1) association of different reactions with different metallic components, (2) association of different reactions with different ensemble sizes of the same metallic component. The former case requires properly selecting the components of the catalyst to expose metal atoms for desirable reactions on active sites. The latter case requires knowledge of detailed structures and microstructures of the bimetallic catalysts. Such detailed microstructural in-

formation is extremely difficult to obtain experimentally, while reliable theoretical predictions require an accurate and computationally efficient model capable of predicting the interplay between number and type of bonding coordination that controls this phenomena.

We have recently introduced a new bond order metal simulator model (BOS-mixing) (8) based upon early work of King and co-worker (9, 10) [called the surface-modified pair potential model (SMPP) by them]. They allowed the metal–metal bond energy to vary with coordination irrespective of type, and allowed an average variation with type (which describes only symmetric mixing curves and makes no distinction between ordered and disordered alloys). Later, DePristo and co-workers (11–16) systematically calculated the metal–metal bond variation with coordination, called the site energy, but neglected any variation with type of neighbor. The parametrization of their model successfully predicted features dominated by the variation of bonding energy with coordination in different metals, e.g., surface segregation due to differences in surface energies (11–16). However, it did not describe the segregation and micromixing caused by variation in the type of metal–metal bond. This limitation was removed in the BOS-mixing model (8) which expressed the site energy of an atom with fixed coordination by a quadratic function of the number of mixed metal bonds.

In the original work of Ref. (8), the BOS-mixing model was parametrized from the mixing energy, dimer bond energy, fcc(111) surface energy, and bulk cohesive energy resulting from the non-self-consistent electron density functional-based corrected effective medium (CEM) theory. The simplest CEM framework was used which neglects the difference in kinetic-exchange-correlation energies between atoms in bulk and surface environments, at the same average electron density. This method is fast enough to use in large-scale molecular dynamics and Monte Carlo simulations and thus has the acronym MD/MC-CEM (17). Since the MD/MC-CEM method was also used to predict the structures of small clusters, the BOS-mixing model was tested rigorously. For the 10 ordered bimetallic alloys formed from Ni, Cu, Rh, Pd, and Ag, only for

a few clusters, e.g., $\text{Ni}_{101}\text{Pd}_{100}$, did the BOS-mixing model display some inaccuracies due to the large size mismatches which distorted the clusters' shapes from the perfect lattice structures.

The mixing energies predicted by CEM and MD/MC-CEM methods are generally not an accurate representation of the experimental mixing energy data (17), and the theoretical values do not exhibit the complication of disordered vs ordered alloy formation which occurs in the experimental data. Since use of accurate mixing data will be crucial to describe real catalysts and to help design new catalysts, in this paper we present the results of using only experimental data to parametrize the BOS-mixing model. The bimetallic systems treated here include all the disordered alloys formed from Ni, Cu, Rh, Pd, Ag, Ir, Pt, and Au. The parametrization of ordered alloys is more complicated and will be presented in another paper (18). As an illustration of the BOS-mixing model, we show microstructures of bimetallic catalysts with 201 atoms and a composition of 50%–50%. Exhaustive studies of the variation of the microstructures with the dispersion, composition, and presence of adsorbates will be discussed in another paper (19). Although all these studies are carried on perfect lattice structures, it is important to mention that the size effect can be included approximately by using a short-time molecular dynamics simulation after the cluster mixing arrangement is determined, as will be illustrated by comparison to experimental X-ray diffraction spectra of $\text{Cu}_x\text{Pd}_{1-x}$ clusters (20).

II. THEORY

A complete derivation of the BOS-mixing model was provided in Ref. (8). We merely state the results here, and refer the interested reader to that article for details. For a system of N atoms, $\{\mathbf{A}_i, i = 1, \dots, N\}$ of two types ("A" or "B"), the interaction energy was expressed as a sum of the site energies,

$$\Delta E(\{\mathbf{A}_i\}) = \sum_{i=1}^N \varepsilon_{Z_i, M_i \text{ of } \beta_i}^{\alpha_i} \quad [1]$$

where α_i and β_i are either A-type or B-type atoms. N is the total number of atoms in the system. Z_i and M_i are the coordination number (i.e., number of nearest neighbors) and the number of unlike atoms around a central atom of type α_i . The site energy for an A-type atom surrounded by M of B-type and $Z-M$ of A-type is written explicitly as

$$\varepsilon_{Z, M \text{ of } \mathbf{B}}^{\mathbf{A}} = \varepsilon_Z^{\mathbf{A}} + M \Delta E_{Z, \mathbf{A}-\mathbf{B}}^{\mathbf{A}} + \frac{M(M-1)}{2} \lambda_{Z, \mathbf{A}-\mathbf{B}}^{\mathbf{A}} \quad [2]$$

where $\varepsilon_Z^{\mathbf{A}}$ is the interaction energy for a Z -coordinated A-type atom with all A-type neighbors, $\Delta E_{Z, \mathbf{A}-\mathbf{B}}^{\mathbf{A}}$ is the

energy change of the first A–B vs A–A bond, and $\lambda_{Z, \mathbf{A}-\mathbf{B}}^{\mathbf{A}}$ is the incremental variation in A–B bond. An analogous expression for a B type atom is

$$\varepsilon_{Z, M \text{ of } \mathbf{A}}^{\mathbf{B}} = \varepsilon_Z^{\mathbf{B}} + M \Delta E_{Z, \mathbf{A}-\mathbf{B}}^{\mathbf{B}} + \frac{M(M-1)}{2} \lambda_{Z, \mathbf{A}-\mathbf{B}}^{\mathbf{B}} \quad [3]$$

Since the site energy depends on the chemical identity of nearest neighbors, the interaction energy of the system is changed by switching the positions of two unlike atoms with the same coordination number. Thus, the alloy heat of formation or mixing energy (ΔE_{mix}) does not necessarily vanish.

Six parameters are required to implement Eqs. [1]–[3] for a binary alloy: site energies of homogenous system, $\varepsilon_1^{\mathbf{A}}$ and $\varepsilon_9^{\mathbf{B}}$, and mixing parameters, $\Delta E_{Z, \mathbf{A}-\mathbf{B}}^{\mathbf{A}}$, $\Delta E_{Z, \mathbf{A}-\mathbf{B}}^{\mathbf{B}}$, $\lambda_{Z, \mathbf{A}-\mathbf{B}}^{\mathbf{A}}$, and $\lambda_{Z, \mathbf{A}-\mathbf{B}}^{\mathbf{B}}$. The site energies of homogenous systems are determined from experimental data following Ref. (16). For $Z=1$, an atom has one nearest neighbor and thus $\varepsilon_1^{\mathbf{A}} = -D_0/2$, where D_0 is the experimental dimer dissociation energy. For $Z=9$, an atom has nine nearest neighbors and thus $\varepsilon_9^{\mathbf{A}}$ is set equal to the interaction energy of an atom in the top layer of the (111) surface. This is just the sum of the bulk cohesive energy, $-E_{\text{coh}}$, and the surface energy at 0 K, $\sigma(111)$, multiplied by the area per atom, on the (111) surface, $(\sqrt{3}/4)a_0^2$ where a_0 is the lattice constant. Most experimental surface energies were taken from Ref. (21) and extrapolated to 0 K (22), except those for Ir and Au, which were taken from Ref. (23). Finally, for $Z=12$, an atom has 12 nearest neighbors and thus $\varepsilon_{12}^{\mathbf{A}} = -E_{\text{coh}}$. It was found that these three data fall almost on a straight line for most metals (16), indicating that a simple linear dependence can be used to express the variation of the site energies with coordination ($1 \leq Z \leq 12$):

$$\varepsilon_Z^{\mathbf{A}} = \begin{cases} \varepsilon_1^{\mathbf{A}} + (\varepsilon_9^{\mathbf{A}} - \varepsilon_1^{\mathbf{A}}) \cdot \frac{(Z-1)}{8} & 1 \leq Z \leq 9 \\ \varepsilon_9^{\mathbf{A}} + (\varepsilon_{12}^{\mathbf{A}} - \varepsilon_9^{\mathbf{A}}) \cdot \frac{(Z-9)}{3} & 9 \leq Z \leq 12. \end{cases} \quad [4]$$

To obtain the four remaining mixing parameters, we utilize experimental mixing energies for the bulk systems at compositions of $\text{A}_{1/32}\text{B}_{31/32}$, $\text{A}_{1/4}\text{B}_{3/4}$, $\text{A}_{1/2}\text{B}_{1/2}$, $\text{A}_{3/4}\text{B}_{1/4}$, and $\text{A}_{31/32}\text{B}_{1/32}$ (23, 24). For a disordered bimetallic alloy formed in the reaction, $x\mathbf{A} + (1-x)\mathbf{B} \rightarrow \mathbf{A}_x\mathbf{B}_{1-x}$, the mixing energy (per atom) as calculated from $\Delta E_{\text{mix}} = E(\mathbf{A}_x\mathbf{B}_{1-x}) - xE(\mathbf{A}) - (1-x)E(\mathbf{B})$ is given as the above five compositions by

$$\begin{aligned} \Delta E_{\text{mix}}(\text{A}_{1/32}\text{B}_{31/32}) &= \frac{3}{8}(\Delta E_{12, \mathbf{A}-\mathbf{B}}^{\mathbf{A}} + \Delta E_{12, \mathbf{A}-\mathbf{B}}^{\mathbf{B}}) \\ &+ \frac{33}{16} \lambda_{12, \mathbf{A}-\mathbf{B}}^{\mathbf{A}} \end{aligned} \quad [5a]$$

$$\begin{aligned}\Delta E_{\text{mix}}(A_{1/4}B_{3/4}) &= \frac{9}{4}(\Delta E_{12, A-B}^A + \Delta E_{12, A-B}^B) \\ &+ (9\lambda_{12, A-B}^A + \frac{9}{4}\lambda_{12, A-B}^B) \quad [5b]\end{aligned}$$

$$\begin{aligned}\Delta E_{\text{mix}}(A_{1/2}B_{1/2}) &= 3(\Delta E_{12, A-B}^A + \Delta E_{12, A-B}^B) \\ &+ \frac{15}{2}(\lambda_{12, A-B}^A + \lambda_{12, A-B}^B) \quad [5c]\end{aligned}$$

$$\begin{aligned}\Delta E_{\text{mix}}(A_{3/4}B_{1/4}) &= \frac{9}{4}(\Delta E_{12, A-B}^A + \Delta E_{12, A-B}^B) \\ &+ \left(\frac{9}{4}\lambda_{12, A-B}^A + 9\lambda_{12, A-B}^B\right) \quad [5d]\end{aligned}$$

$$\begin{aligned}\Delta E_{\text{mix}}(A_{31/32}B_{1/32}) &= \frac{3}{8}(\Delta E_{12, A-B}^A + \Delta E_{12, A-B}^B) \\ &+ \frac{33}{16}\lambda_{12, A-B}^B. \quad [5e]\end{aligned}$$

This can be written in convenient matrix–vector notation as

$$\Delta \mathbf{E}_{\text{mix}} = \mathbf{C}_{\text{disorder}} \mathbf{P}, \quad [6]$$

where the individual matrices and vectors are

$$\Delta \mathbf{E}_{\text{mix}} = \begin{pmatrix} \Delta E_{\text{mix}}(A_{1/32}B_{31/32}) \\ \Delta E_{\text{mix}}(A_{1/4}B_{3/4}) \\ \Delta E_{\text{mix}}(A_{1/2}B_{1/2}) \\ \Delta E_{\text{mix}}(A_{3/4}B_{1/4}) \\ \Delta E_{\text{mix}}(A_{31/32}B_{1/32}) \end{pmatrix} \quad [7]$$

$$\mathbf{C}_{\text{disorder}} = \begin{pmatrix} 3/8 & 33/16 & 0 \\ 9/4 & 9 & 9/4 \\ 3 & 15/2 & 15/2 \\ 9/4 & 9/4 & 9 \\ 3/8 & 0 & 33/16 \end{pmatrix} \quad [8]$$

$$\mathbf{P} = \begin{pmatrix} \Delta E_{12, A-B}^A + \Delta E_{12, A-B}^B \\ \lambda_{12, A-B}^A \\ \lambda_{12, A-B}^B \end{pmatrix}. \quad [9]$$

Note that the energies of formation are actually functions of three parameters, $\Delta E_{12, A-B}^A + \Delta E_{12, A-B}^B$, $\lambda_{12, A-B}^A$, and $\lambda_{12, A-B}^B$. Although these three parameters are (over)determined, in principle, by these five experimental mixing energies, the parametrization procedure is complicated due to lack of knowledge about both the degree of disorder of the alloy and the measurement uncertainty. A detailed description of the fitting procedure is contained in the next section. Finally, once the parameter $\Delta E_{12, A-B}^A + \Delta E_{12, A-B}^B$ is known, the individual components

of $\Delta E_{Z, A-B}^A$ and $\Delta E_{Z, A-B}^B$ with any coordination Z is provided by the relationship (8),

$$\Delta E_{Z, A-B}^A = \frac{\Delta E_{12, A-B}^A + \Delta E_{12, A-B}^B}{2} - \frac{(\varepsilon_Z^A - \varepsilon_Z^B)}{2Z} \quad [10a]$$

$$\Delta E_{Z, A-B}^B = \frac{\Delta E_{12, A-B}^A + \Delta E_{12, A-B}^B}{2} + \frac{(\varepsilon_Z^A - \varepsilon_Z^B)}{2Z}. \quad [10b]$$

The dependence of $\Delta E_{Z, A-B}^A + \Delta E_{Z, A-B}^B$, $\lambda_{Z, A-B}^A$, and $\lambda_{Z, A-B}^B$ on Z is neglected, or in mathematical terms

$$\Delta E_{Z, A-B}^A + \Delta E_{Z, A-B}^B = \Delta E_{12, A-B}^A + \Delta E_{12, A-B}^B \quad [11a]$$

$$\lambda_{Z, A-B}^A = \lambda_{12, A-B}^A \quad [11b]$$

$$\lambda_{Z, A-B}^B = \lambda_{12, A-B}^B. \quad [11c]$$

With all four parameters, we can apply the BOS-mixing model to calculate the energy of any geometrical arrangement of the atoms.

III. DETERMINATION OF MIXING PARAMETERS

In Table 1, the experimental mixing enthalpies and measurement temperature are shown for the 10 binary bulk alloys formed from Ni, Cu, Rh, Pd, Ag, Ir, Pt, Ir, and Au which have positive or small negative mixing enthalpies (23, 24). We do not consider alloys with a large negative enthalpy of mixing since these are likely either to be ordered or to exhibit domains of disorder and order. Ordered systems will be presented in another paper (18) in which the SCF-DFT calculated values for the ordered systems are used to judge the ordering degree in the experimental data. The experimental mixing energies are set equal to the enthalpies since the difference between ΔH_{mix} and ΔE_{mix} is typically on the order of only 1–2 kJ/mol even at 1000 K for solids.

Note that three alloys, Ni–Cu, Ni–Au, and Cu–Ag, have positive mixing energies at all five compositions. A different type of mixing energy curve is displayed by Ni–Pd which is positive at Ni-rich and negative at Pd-rich compositions. Finally, six alloys, Ni–Rh, Cu–Rh, Rh–Pd, Rh–Ir, Pd–Pt, and Ir–Pt, have information at only one composition, $A_{1/2}B_{1/2}$, which is positive for Ni–Rh, Cu–Rh, Rh–Pd, and Rh–Ir alloys, and negative for Pd–Pt and Ir–Pt alloys.

The three parameters in Eq. [9] are determined by a general approach including model applicability, structure testing, data fitting, and error analysis. First, we analyze the data to ensure the applicability of the BOS model, i.e., to discover the structures contained within the data. To do this, we note that using the equations either for disordered alloys in Eq. [5] or for ordered alloys in Ref. (8), the following relationship holds:

$$\frac{2[\Delta E(A_{1/4}B_{3/4}) + \Delta E(A_{3/4}B_{1/4})]}{3\Delta E(A_{1/2}B_{1/2})} = 1. \quad [12]$$

TABLE 1

Mixing Energies (kJ/mol) for Bimetallic Alloys, A_xB_{1-x} , as a Function of Composition

A–B	Experimental values (input)					T (K)	Ref.	BOS-mixing model (output) ^a					σ_{RMS}^b	Q^c
	0.031	0.25	0.50	0.75	0.969			0.031	0.25	0.50	0.75	0.969		
Ni–Cu	0.10	0.90	1.78 ± 0.42	1.73	0.30	973	20	0.10	0.95	1.71	1.62	0.30	0.07	0.62
Ni–Rh			1.1			1100	21	0.14	0.83	1.10	0.83	0.14	—	—
Ni–Pd	–0.26	–1.18	$–0.54 \pm 1.26$	0.48	0.17	1273	20	–0.27	–1.08	–0.47	0.39	0.18	0.08	0.019
Ni–Au	0.65	4.82	7.56 ± 0.42	5.89	0.84	1150	20	0.65	5.10	7.23	5.74	0.84	0.23	0.74
Cu–Rh			5.8			1500	21	0.73	4.35	5.80	4.35	0.73	—	—
Cu–Ag	0.59	3.49	4.24 ± 0.21	3.05	0.46	1423	20	0.52	3.10	4.13	3.10	0.52	0.21	0.0087
Rh–Pd			10			1575	21	1.25	7.50	10.00	7.50	1.25	—	—
Rh–Ir			2			1461	21	0.25	1.50	2.00	1.50	0.25	—	—
Pd–Pt			–3.6			298	21	–0.45	–2.70	–3.60	–2.70	–0.45	—	—
Ir–Pt			–3			1478	21	–0.38	–2.25	–3.00	–2.25	–0.38	—	—

^a From Eq. [5] using the parameters in Table 2.^b RMS deviation defined as $\sqrt{\frac{\sum_{i=1}^5 [\Delta E_{\text{mix}}^{\text{output}}(A_{x_i}B_{1-x_i}) - \Delta E_{\text{mix}}^{\text{input}}(A_{x_i}B_{1-x_i})]^2}{5-1}}$.^c The goodness-of-fit estimated with the probability that the observed χ^2 exceed the value of χ^2 obtained in fitting procedure by chance, $Q(\frac{v}{2}, \frac{\chi^2}{2})$ where v is 2 for Ni–Cu, Ni–Pd, and Ni–Au and 4 for Cu–Ag.

For Ni–Cu, Ni–Pd, Ni–Au, and Cu–Ag this ratio is 0.99, 0.86, 0.94, and 1.03, respectively. With the possible exception of Ni–Pd, the BOS model is consistent with the data structure. Second, we analyze the data to determine if the alloys are disordered. To do this, we note that using the equations for ordered alloys in Ref. (8) along with Eq. [5] yields the relationship

$$\frac{\Delta E_{\text{mix}}(A_{1/4}B_{3/4}) - \Delta E_{\text{mix}}(A_{3/4}B_{1/4})}{\Delta E_{\text{mix}}(A_{1/32}B_{31/32}) - \Delta E_{\text{mix}}(A_{31/32}B_{1/32})} = \begin{cases} 36/11 \approx 3.3 & \text{disordered} \\ 64/11 \approx 5.8 & \text{ordered.} \end{cases} \quad [13]$$

For Ni–Cu, Ni–Pd, Ni–Au, and Cu–Ag, this ratio is 4.1, 3.9, 5.7, and 3.4, respectively. Thus, the Ni–Cu, Ni–Pd, and Cu–Ag systems are apparently disordered while Ni–Au system might be ordered. However, we still consider it in this paper since we have found that microstructure of $\text{Ni}_{101}\text{Au}_{100}$ is the same irrespective of whether ordered or disordered parameters are used. This is true only when the system has a positive mixing energy that is not too large compared to the surface energy difference.

Next, we turn to fitting of the cases with five experimental mixing energies by least square minimization of the quantity

$$\chi^2 = \sum_{i=1}^5 \left(\frac{\Delta E_{\text{mix-expt}}^i - \Delta E_{\text{mix-BOS}}^i}{\sigma_i} \right)^2, \quad [14]$$

which is a sum of five squares of normally distributed quantities, each normalized to unit variance. Here, $\Delta E_{\text{mix-expt}}^i$ is

the experimental mixing energy at each of the five compositions, $\Delta E_{\text{mix-BOS}}^i$ is the BOS mixing energy at the same composition, and σ_i is the measurement error associated with experimental datum, $\Delta E_{\text{mix-expt}}^i$. Minimization of Eq. [14] yields the solution (25) for the best-fit parameters:

$$\mathbf{P} = (\mathbf{C}_{\text{disorder}}^T \cdot \mathbf{s}^{-2} \cdot \mathbf{C}_{\text{disorder}})^{-1} \cdot \mathbf{C}_{\text{disorder}}^T \cdot \mathbf{s}^{-2} \cdot \Delta \mathbf{E}_{\text{mix-expt}}, \quad [15]$$

where \mathbf{P} is the 3×1 vector in Eq. [9] and

$$\mathbf{s} = \begin{pmatrix} \sigma_1 & 0 & 0 & 0 & 0 \\ 0 & \sigma_2 & 0 & 0 & 0 \\ 0 & 0 & \sigma_3 & 0 & 0 \\ 0 & 0 & 0 & \sigma_4 & 0 \\ 0 & 0 & 0 & 0 & \sigma_5 \end{pmatrix} \quad [16]$$

is the diagonal matrix of experimental uncertainties.

There is little knowledge about these uncertainties except at a composition of $A_{1/2}B_{1/2}$, where some information exists from comparison of mixing energies obtained either in different laboratories or by two or more methods which differ in principle (24). As listed in Table 1, Ni–Cu and Ni–Pd alloys have large measurement errors of 24 and 233%, respectively, while Cu–Ag is much smaller at 5.0%. Such errors make little sense since the temperatures and mixing energies are quite comparable in all four systems. To estimate the adequacy of the BOS-mixing model and to determine the accuracy of the parameters, we use an average relative deviation of 10% at all compositions except for the impurities ($A_{1/32}B_{31/32}$ and $A_{31/32}B_{1/32}$) which are assumed

TABLE 2
BOS-Mixing Model Parameters (kJ/mol)^a

A-B	$\Delta E_{12,A-B}^A +$		$\Delta E_{12,A-B}^B$		$\lambda_{12,A-B}^A$		$\lambda_{12,A-B}^B$		Cov $(\lambda_{12,A-B}^A, \lambda_{12,A-B}^B)$		Cov $(\lambda_{12,A-B}^B, \lambda_{12,A-B}^B)$		Cov $(\lambda_{12,A-B}^A, \lambda_{12,A-B}^B)$	
	$\Delta E_{12,A-B}^A$	$\Delta E_{12,A-B}^B$	$\Delta E_{12,A-B}^A$	$\Delta E_{12,A-B}^B$	$\lambda_{12,A-B}^A$	$\lambda_{12,A-B}^B$	$\Delta E_{12,A-B}^A + \Delta E_{12,A-B}^B$	$\Delta E_{12,A-B}^A + \Delta E_{12,A-B}^B$	$\Delta E_{12,A-B}^A + \Delta E_{12,A-B}^B$	$\Delta E_{12,A-B}^A + \Delta E_{12,A-B}^B$	$\Delta E_{12,A-B}^A + \Delta E_{12,A-B}^B$	$\Delta E_{12,A-B}^A + \Delta E_{12,A-B}^B$	$\Delta E_{12,A-B}^A + \Delta E_{12,A-B}^B$	
Ni-Cu	0.91 ± 0.37	4.27 ± 0.37	-3.36 ± 0.37	-0.12 ± 0.07	-0.02 ± 0.07		-0.026		-0.027		0.005			
Ni-Rh	0.37	-5.08	5.45	0.0	0.0		—		—		—			
Ni-Pd	-0.14 ± 0.24	2.01 ± 0.24	-2.42 ± 0.24	-0.06 ± 0.05	0.16 ± 0.05		-0.012		-0.011		0.002			
Ni-Au	6.61 ± 1.67	5.84 ± 1.67	0.77 ± 1.67	-0.89 ± 0.31	-0.79 ± 0.31		-0.517		-0.520		0.096			
Cu-Rh	1.93	-8.12	10.05	0.0	0.0		—		—		—			
Cu-Ag	1.38 ± 0.04	2.86 ± 0.04	-1.48 ± 0.04	0.0	0.0		—		—		—			
Rh-Pd	3.33	9.14	-5.81	0.0	0.0		—		—		—			
Rh-Ir	0.67	-4.45	5.12	0.0	0.0		—		—		—			
Pd-Pt	-1.20	-8.44	7.24	0.0	0.0		—		—		—			
Ir-Pt	-1.00	3.92	-4.92	0.0	0.0		—		—		—			

^a ε_{12}^A values are -4.44 , -3.49 , -5.75 , -3.89 , -2.95 , -6.94 , -5.84 and -3.81 eV for Ni, Cu, Rh, Pd, Ag, Ir, Pt, and Au, respectively (16). $\lambda_{Z,A-B}^A = 0$ are assumed in the fitting for Ni-Rh, Cu-Rh, Cu-Ag, Rh-Pd, Rh-Ir, Pd-Pt, and Ir-Pt. See the text for details.

accurate to 5%. The smaller relative deviations for the impurity data reflect both the ease of such measurements and the agreement between the ordered and disordered model for such low concentrations.

Using standard error analysis with the above uncertainties, the BOS-mixing parameters and uncertainties were found as displayed in Table 2. The variance (squared uncertainty) of the fitted parameters and the covariance between each pair of parameters are directly obtained from the appropriate diagonal and off-diagonal elements of the matrix $(\mathbf{C}_{\text{disorder}}^T \cdot \mathbf{s}^{-2} \cdot \mathbf{C}_{\text{disorder}})^{-1}$, respectively. In addition, the goodness-of-fit of the data and RMS deviation are reported in Table 1. The former is estimated by the standard χ^2 test, requiring evaluation of the incomplete gamma function of $Q(\frac{v}{2}, \frac{\chi^2}{2})$ in which v is the number of degrees of freedom. If Q is larger than ≈ 0.1 , then the fit is quite believable. If it is smaller than ≈ 0.1 but larger than ≈ 0.001 , then the fit may be acceptable. If Q is less than ≈ 0.001 then the model and/or estimation procedure is questionable (25).

From Tables 1 and 2, it is apparent that the BOS-mixing model is excellent for Ni-Cu and Ni-Au, and quite acceptable for Ni-Pd. For Cu-Ag, the experimental mixing energies are very symmetric with the variation from $x=1/32$ to $31/32$, nearly equal to that of the coefficient of $\Delta E_{12,A-B}^A + \Delta E_{12,A-B}^B$ in Eq. [5], i.e., $1:6:8:6:1$. This makes it impossible to extract the parameters $\lambda_{12,A-B}^A$ and $\lambda_{12,A-B}^B$ without large statistical correlation between these and the $\Delta E_{12,A-B}^A + \Delta E_{12,A-B}^B$. Since the former will be small for this case, we have fixed $\lambda_{12,A-B}^A$ and $\lambda_{12,A-B}^B$ at zero for the Cu-Ag alloy. Under this approximation, the standard deviation of fitting is slightly increased (from 0.05 to 0.21 kJ/mol), but it is still reasonably small. From this case, one can clearly see that the fitting procedure offers

a compromise between model complexity and uncertainty. In general, the agreement between the experimental mixing energies and BOS-mixing energies, which are calculated with the parameters in Table 2, is obvious. The BOS-mixing model describes well not only symmetric mixing energy curves, e.g., Cu-Ag, but also asymmetric mixing energy curves, e.g., Ni-Pd.

There are six alloys, Ni-Rh, Cu-Rh, Rh-Pd, Rh-Ir, Pd-Pt, and Ir-Pt, which do not follow the procedure described above. Due to insufficient knowledge about the mixing energy for these alloys, it is not possible either to evaluate the ordering or disordering of the alloy structure or to determine the three BOS parameters. An approximate approach is to assume a disordered structure, since the mixing energies are small, and to let the two parameters, $\lambda_{12,A-B}^A$ and $\lambda_{12,A-B}^B$, be zero. Therefore, the parameter of $\Delta E_{12,A-B}^A + \Delta E_{12,A-B}^B$ is directly derived from Eq. [5c]. In the event that the systems were really ordered analogous to the Ni-Pt one, the parameter $\Delta E_{12,A-B}^A + \Delta E_{12,A-B}^B$ would be reduced by a factor of 3/4 but the coefficients for nearly all situations in clusters would also be increased by a similar factor, leading to negligible net change. Thus, there would be very little difference in mixing behaviors for these systems since the bulk-surface segregation is controlled by the significant surface energy differences while the micromixing on the surface is controlled by the sign of the mixing energy, which is the same irrespective of whether ordered or disordered analysis is used. We emphasize that this is the case only when the $\lambda_{12,A-B}^A$ and $\lambda_{12,A-B}^B$ are set to zero.

Browsing through the results in Table 2, we notice that the two mixing parameters, $\lambda_{12,A-B}^A$ and $\lambda_{12,A-B}^B$, differ substantially for the two systems with large asymmetric mixing energies, e.g., Ni-Cu and Ni-Pd. For the Ni-Pd system, the

two parameters differ even in sign, indicating that the Ni atom prefers to bind with large numbers of Pd atoms while Pd atoms do not prefer to bond with large numbers of Ni atoms. This system also demonstrates that the quadratic term in Eqs. [2] and [3] cannot be neglected since the variation of mixed bond strength with the number of mixed bonds can have important physical consequences.

IV. APPLICATION TO MICROSTRUCTURES OF BIMETALLIC CLUSTERS

We used the BOS-mixing model with the parameters in Table 2 to predict the microstructures of bimetallic clusters, $A_{101}B_{100}$. The perfect cubo-octahedral structure is used, which has a 61% dispersion with 122 surface atoms. Of these 122, there are 24, 36, 6, and 56 atoms occupying the corner, edge, fcc(100), and fcc(111) sites, respectively, and having 6-, 7-, 8-, and 9-fold coordination, respectively. We initialized the bimetallic clusters with all 79 bulk sites occupied by the atoms with higher surface energy and with the remaining 122 atoms randomly occupying the surface sites. To find the equilibrium distribution, pairs of atoms of different type were switched in the lattice, the system energy change was computed, and the standard Monte Carlo prescription for retention of configurations was invoked.

The microstructures of bimetallic clusters, i.e., segregation to surface, edge, and corner sites and micromixing on the surface, are controlled by various physical and chemical factors. The four main contributions include: (i) the difference of surface energies (i.e., the energy difference between the surface and bulk sites, as shown in Table 3); (ii) the mixing energy; (iii) the entropy; (iv) the atomic size difference. The first two quantities are incorporated into the parameters of the BOS-mixing model. The third quantity (entropy) is included in the Monte Carlo simulations. The last quantity (size effect) is not included in the BOS model. If there is a large size mismatch of two elements (which prevents optimal separation for both types), this forces a deviation

from the BOS-predicted results: the atoms of larger size will tend to be expelled to surfaces (15). We expect this to be a rather small effect except in the case of very large size mismatch, such as Ni–Ag or Ni–Au, and even in this case, the cubo-octahedral shape has been found to be a reasonable representative for real catalysts (26, 27).

With neglect of size effects in the BOS model, we can identify the characteristic behavior of each of the three other factors. The difference of surface energy always causes segregation of the atoms with lower surface energy to the lower coordinated sites, most obviously leading to surface enrichment of the atoms with lower surface energy. The mixing energy effect depends upon the sign: for positive values atoms favor having neighbors of the same type, while for negative values atoms favor having neighbors of the other type. The entropy term always favors mixing of atoms of different types. The microstructure of a cluster results from competition among these three terms. Sometimes one term may be so much larger than the others as to dominate the microstructure and thus make the prediction of the microstructure rather simple.

To obtain an idea of the sizes of these terms and to describe the simplistic analysis that is often possible, we present the surface energies in Table 3. The reader should note that typical surface energy difference for fcc(111) sites are 5–40 kJ/mol in magnitude. For comparison, the mixing energies in Table 1 are generally 2–8 kJ/mol in magnitude, while the entropy of mixing is such that $T\Delta S$ has a value of 5.8 kJ/mol at 1000 K for an ideal binary 50%–50% mixture. The most common situation will involve dominance by the surface energy difference in which the characteristic behavior is segregation of the low surface energy atom to the surface. The secondary behavior is surrounding of a surface atom by the same type of atom for positive mixing energy and different type of atom for negative mixing energy. A tertiary behavior is the increase of mixing with temperature due to entropy.

We provide a detailed analysis of overall surface segregation for 10 of the alloys in Table 4. The surface sites include all nonbulk sites, i.e., the corner, edge, fcc(100), and fcc(111) sites. At 0 K, where the effect of entropy vanishes, we notice that systems can be divided into two classes. The first has small positive or negative mixing energies and includes Ni–Cu, Ni–Rh, Ni–Au, Cu–Rh, Cu–Ag, Rh–Pd, Rh–Ir, Pd–Pt, and Ir–Pt. The surface segregation of these alloys is dominated by the differences of surface energies, as is evident from Table 4. All 79 bulk sites are occupied by the type of atom with higher surface energy, except for the Pd–Pt system in which three Pd atoms of lower surface energy occupy these bulk sites. Thus, the first element occupies 18% of surface sites if it has higher surface energy or 83% of surface sites (80% for Pd–Pt) if it has lower surface energy. The second class of alloy, with Ni–Pd as the only example, has moderate negative mixing energies, at Pd-rich

TABLE 3

“Surface Energy” (kJ/mol) at fcc(111), fcc(100), Edge, Corner Sites in the 201-Atom Clusters^a

	σ (111)	σ (100)	σ (edge)	σ (corner)
Ni	80.1	111.0	141.8	172.7
Cu	69.5	90.7	111.9	133.1
Rh	111.0	148.6	186.2	224.8
Pd	85.9	115.8	145.7	175.6
Ag	59.8	78.2	95.5	113.9
Ir	115.8	163.1	209.4	256.7
Pt	100.3	139.9	178.5	218.1
Au	65.6	89.7	112.9	137.0

^aThe surface energy is defined as $\varepsilon_Z - \varepsilon_{12}$, where ε_Z is the site energy and $Z = 9, 8, 7$, and 6 for (111), (100), edge, and corner sites, respectively.

TABLE 4

Data and Results on 201-Atom Bimetallic Clusters

A-B	Surface energy (kJ/mol) [$\sigma(111; A) - \sigma(111; B)$]	Mixing energy (kJ/mol) [$\Delta E_{\text{mix}}(1/2, 1/2)$]	% of surface sites occupied by "A"		
			0 K	300 K	1000 K
Ni-Cu	11	1.8	18	18	24
Ni-Rh	-31	1.1	83	83	81
Ni-Pd	-6	-0.54	43	44	49
Ni-Au	15	7.6	18	20	28
Cu-Rh	-42	5.8	83	83	83
Cu-Ag	10	4.2	18	18	28
Rh-Pd	25	10	18	18	18
Rh-Ir	-5	2	83	83	74
Pd-Pt	-14	-3.6	80	79	74
Ir-Pt	16	-3	18	21	29

compositions, which compete with the difference of surface energy in controlling of microstructure of Ni-Pd. As a result, 49 Ni atoms of smaller surface energy enter bulk sites to replace Pd atoms, causing overall surface segregation of Ni to decrease to 43%. Such an effect could not have been predicted without the quantitative BOS-mixing model.

The influence of entropy on the microstructure is clearly seen from the variation of surface segregation with the temperature in Table 4. For every system, the mixing increases with increasing temperature, although the amount depends sensitively on the surface energy difference compared to $T\Delta S$. For systems such as Ni-Rh, Cu-Rh, and Rh-Pd, the surface energy difference is easily five times $T\Delta S$ even at 1000 K and the effect of entropy is negligible. For the other systems, the mixing increases quite substantially by 1000 K.

Displayed in Figs. 1 and 2 are two prototypical alloys, Ni-Cu and Ir-Pt, at 0 K. Both alloys exhibit similar surface-bulk segregation (i.e., interior sites are occupied by the type of atoms having higher surface energy). However, they display opposite microstructures on the surfaces with segregation of the two types of atoms in Ni-Cu and mixing in Ir-Pt.

A more sophisticated analysis of surface compositions for all 10 alloys is displayed in Table 5. The number of unlike surface neighbors is obtained by counting the surface neighbors of different type than the central surface atom. We notice that at 0 K the element having higher surface energy and occupying fcc(111) site has an average of 2.4–2.7 surface neighbors of the other type for the alloys with positive mixing energy. However, for the alloys with negative mixing energy the element has 6 unlike surface neighbors. At high temperatures, both kinds of systems tend to have an equal number of unlike surface neighbors, which is close to the random distribution.

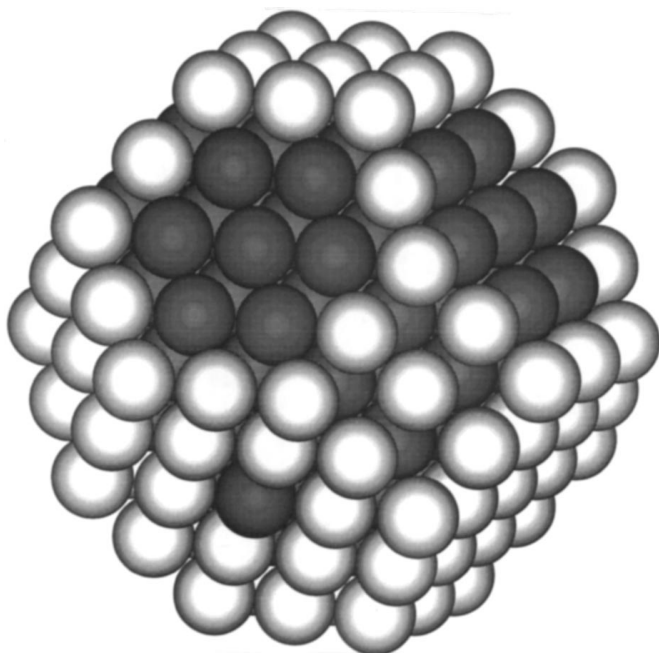


FIG. 1. The lowest-energy configuration for $\text{Ni}_{101}\text{Cu}_{100}$ at 0 K predicted by the BOS-mixing model. The first metal is shown as a dark sphere and the second as a light sphere.

V. CONCLUSIONS

We parametrized the bond order metal simulator model (BOS-mixing model) in this paper for 10 disordered alloys formed from Ni, Cu, Rh, Pd, Ag, Ir, Pt, and Au. In the

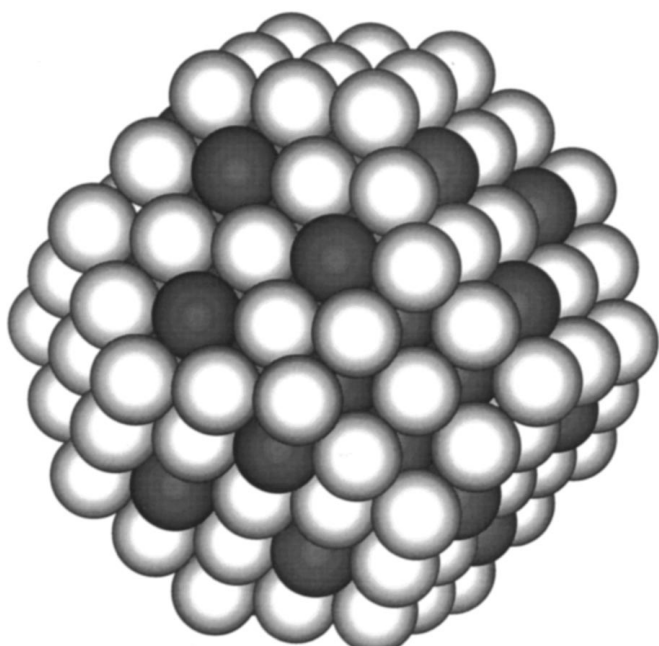


FIG. 2. Same as Fig. 1 but for $\text{Ir}_{101}\text{Pt}_{100}$.

TABLE 5

The Percentage of fcc(111) Sites Occupied by the Element with Higher Surface Energy in the 201-Atom Bimetallic Catalysts and Their Averaged Unlike Surface Neighbors

A-B	0 K		300 K		1000 K	
	%	Unlike neighbor	%	Unlike neighbor	%	Unlike neighbor
Ni-Cu	39	2.7	39	4.4	43	4.3
Ni-Rh	38	2.6	37	4.7	35	4.7
Ni-Pd	7	6.0	25	3.3	41	3.0
Ni-Au	39	2.7	40	3.3	47	3.7
Cu-Rh	38	2.6	38	3.5	37	4.4
Cu-Ag	38	2.4	38	3.8	39	3.8
Rh-Pd	39	2.7	39	2.8	37	4.1
Rh-Ir	38	2.6	38	4.4	49	4.1
Pd-Pt	43	6.0	47	5.1	52	4.4
Ir-Pt	39	6.0	45	5.0	50	4.2

BOS model, the variation of metal–metal bond strength with number and type of atomic neighbors is described using a quadratic form. The variation with coordination for homogeneous systems was taken from previous work (15) which used the experimental dimer binding energies, surface energies, and cohesive energies. The variation with type of neighbor was determined in this paper by fitting the experimental mixing energies as a function of composition for bulk bimetallic systems. First, we determined that the experimental data was consistent with the BOS model for disordered bulk alloys. Then, to implement the fitting, we used the weighted least squares technique including error propagation and analysis. All best-fitted parameters are accompanied by their uncertainties.

Using these parameters, the BOS-mixing model was used to predict microstructures of bimetallic clusters at a size of 201 atoms (60% dispersion) and a composition of 50%–50%. These microstructures included the overall surface segregation as well as the detailed segregation to different sites and micromixing. We have found that three effects determine the microstructures: the difference of surface energies, mixing energy, and entropy. All these studies were performed on the perfectly shaped cubo-octahedral structures neglecting any size effect. It has been noticed that the size effect can be included by introducing a short-time molecular dynamics annealing of the BOS-determined structure, and this will be reported in future work comparing experimental data on cluster shape and structure (20). However, we do emphasize that even without this modification the BOS-mixing model can be used to provide use-

ful information about microstructures for many bimetallic clusters.

ACKNOWLEDGMENTS

This work was supported by the Office of Industrial Technology, Energy Efficiency Division, U.S. Department of Energy, through the Ames Laboratory, which is operated for the U.S. DOE by Iowa State University under Contract W-7405-Eng-82.

REFERENCES

1. (a) Sinfelt, J. H., "Bimetallic Catalysts: Discoveries, Concepts and Applications." Wiley, New York, 1983. (b) Sinfelt, J. H., *Acc. Chem. Res.* **20**, 134 (1987). (c) Sinfelt, J. H., *Int. Rev. Phys. Chem.* **7**, 281 (1988).
2. Campbell, C. T., *Annu. Rev. Phys. Chem.* **41**, 775 (1990).
3. Rodriguez, J. A., and Goodman, D. W., *Science* **57**, 897 (1992).
4. Gauthier, Y., Hoffmann, W., and Wuttig, M., *Surf. Sci.* **233**, 239 (1990).
5. van de Riet, E., Deckers, S., Habraken, F. H. P. M., and Niehaus, A., *Surf. Sci.* **243**, 49 (1991).
6. Fasteiger, H. A., Ross, P. N., Jr., and Cairns, E. J., *Surf. Sci.* **293**, 67 (1993).
7. Jacobson, R. L., Kluksdahl, H. E., McCoy, C. S., and Davis, R. W., *Proc. Am. Pet. Inst. Div. Refin.* **49**, 504 (1969).
8. Zhu, L., and DePristo, A. E., *J. Chem. Phys.* **102**, 5342 (1995).
9. King, T. S., in "Automobile Catalytic Converters" (K. C. Taylor, Ed.), Springer, New York, 1984.
10. (a) Strohl, J. K., and King, T. S., *J. Catal.* **116**, 540 (1989). (b) Strohl, J. K., and King, T. S., *J. Catal.* **118**, 53 (1989).
11. Schoeb, A. M., Raeker, T. J., Yang, L., Wu, X., King, T. S., and DePristo, A. E., *Surf. Sci. Lett.* **278**, L125 (1992).
12. Yang, L., Raeker, T. J., Schoeb, A. M., Wu, X., King, T. S., and DePristo, A. E., *Am. Chem. Soc. Div. Fuel. Chem.* **37**, 324 (1992).
13. Yang, L., Raeker, T. J., and DePristo, A. E., *Surf. Sci.* **290**, 195 (1993).
14. Yang, L., and DePristo, A. E., *J. Chem. Phys.* **100**, 725 (1994).
15. Yang, L., and DePristo, A. E., *J. Catal.* **148**, 575 (1994).
16. Yang, L., and DePristo, A. E., *J. Catal.* **149**, 223 (1994).
17. Raeker, T. J., and DePristo, A. E., *Phys. Rev. B* **49**, 8663 (1994).
18. Zhu, L., DePristo, A. E., Ruban, A. V., and Skriver, H. L., unpublished data.
19. Zhu, L., Wang, R., King, T., and DePristo, A. E., *J. Catal.* **167**, 408 (1997).
20. Zhu, L., Liang, K. S., Zhang, B., Bradley, J. S., and DePristo, A. E., *J. Catal.* **167**, 412 (1997).
21. Mezey, L. Z., and Giber, J., *Jpn. J. Appl. Phys.* **21**, 1569 (1982).
22. Sinnott, S. B., Stave, M. S., Raeker, T. J., and DePristo, A. E., *Phys. Rev. B* **44**, 8927 (1991).
23. de Boer, F. R., Boom, R., Mattens, W. C. M., Miedema, A. R., and Niessen, A. K., "Cohesion in Metals." North-Holland, Amsterdam, 1988.
24. Hultgren, R., Desai, P. D., Hawkins, D. T., Gleiser, M., and Kelley, K., "Selected Values of the Thermodynamic Properties of Binary Alloys." Univ. Microfilms, Ann Arbor, MI, 1990.
25. Press, W. H., Flannery, B. P., Teukolsky, S. A., and Vetterling, W. T., "Numerical Recipes." Cambridge University Press, New York, 1988.
26. Dominguez, J. M., and Yacaman, M. J., *J. Catal.* **64**, 213 (1980).
27. Yacaman, M. J., and Dominguez, J. M., *J. Catal.* **64**, 223 (1980).